Journal of Solid State Chemistry 182 (2009) 1624–1630

Contents lists available at ScienceDirect

Journal of Solid State Chemistry

journal homepage: www.elsevier.com/locate/jssc

Magnetic properties of EuLn_2O_4 (Ln = rare earths)

Keiichi Hirose, Yoshihiro Doi, Yukio Hinatsu *

Division of Chemistry, Hokkaido University, Sapporo 060–0810, Japan

ARTICLE INFO

Article history:
Received 19 January 2009
Received in revised form
1 April 2009
Accepted 2 April 2009
Available online 9 April 2009

Keywords:
Magnetic properties
Rare earths
Oxides
Antiferromagnetic interactions
Magnetic susceptibility
Mössbauer spectroscopy

ABSTRACT

Ternary rare earth oxides EuLn_2O_4 (Ln = Gd, Dy–Lu) were prepared. They crystallized in an orthorhombic $CaFe_2O_4$-type structure with space group *Pnma*. ^{151}Eu Mössbauer spectroscopic measurements show that the Eu ions are in the divalent state. All these compounds show an antiferromagnetic transition at 4.2–6.3 K. From the positive Weiss constant and the saturation of magnetization for $EuLu_2O_4$, it is considered that ferromagnetic chains of Eu^{2+} are aligned along the *b*-axis of the orthorhombic unit cell, with neighboring Eu^{2+} chains antiparallel. When Ln = Gd–Tm, ferromagnetically aligned Eu^{2+} ions interact with the Ln^{3+} ions, which would overcome the magnetic frustration of triangularly aligned Ln^{3+} ions and the EuLn_2O_4 compounds show a simple antiferromagnetic behavior.

1. Introduction

It is well known that oxides containing rare earth elements show a variety of magnetic properties due to the behavior of unpaired 4*f* electrons. When the rare earth ions are arrayed in a structurally characteristic manner, interesting magnetic behavior has been often found. Here, we focus our attention on a series of EuLn_2O_4 (Ln = rare earths) with the $CaFe_2O_4$-type structure. The smaller cations are located at the centers of anion octahedra which share edges in such a way as to give double chains along *b*-axis. Adjacent double chains of anion octahedra are connected by corners, four of them surrounding a chain of the larger cations. The larger cation then is surrounded by six anions in a trigonal-prismatic arrangement and has another two coplanar anion neighbors.

Compounds EuLn_2O_4 with Ln = Gd, Yb and Lu were reported to reveal magnetic ordering at 4.5, 11 and 9.5 K, respectively [1–3]. $EuDy_2O_4$ showed paramagnetic behavior in the temperature range of 80–800 K through magnetic susceptibility measurements [4]. No further magnetic properties have been investigated. For other EuLn_2O_4 compounds (Ln = Sm, Ho–Tm), the preparation conditions were reported, but no magnetic properties have been known [5]. Attfield determined the valence and cation distribution of $EuSm_2O_4$ by resonant powder X-ray diffraction method [6]. Recently, sulfide and selenide compounds isomorphous with EuLn_2O_4, i.e., EuLn_2S_4 and EuLn_2Se_4 (Ln = Tb–Lu) were studied and the occurrence of the antiferromagnetic transition at 3–4 K was reported [7].

SrLn_2O_4 and BaLn_2O_4 adopt the same structure. Karunadasa et al. measured the magnetic susceptibilities and neutron diffraction profiles on SrLn_2O_4 (Ln = Gd, Dy–Yb) [8]. These compounds indicated the existence of magnetic frustration at around 4 K, which is ascribable to its characteristic structure, i.e., zigzag chains consisting of edge-shared Ln_3 triangles and the honeycomb-like structure formed by the chains. We measured the magnetic susceptibility and specific heat of BaLn_2O_4 (Ln = Pr, Nd, Sm–Ho) and found that they showed an anomaly at 2.2–4.0 K [9]. These magnetic behaviors are due to the magnetic interactions between Ln^{3+} ions, and the alkali earths (Sr or Ba) do not contribute to the magnetism of SrLn_2O_4 or BaLn_2O_4, because they are diamagnetic. By introducing the divalent europium ions Eu^{2+} into the alkali earth sites, such paramagnetic ions with a large magnetic moment should contribute to the magnetic interactions between the Ln^{3+} ions.

In this study, we prepared a series of EuLn_2O_4 compounds (Ln = Gd, Dy–Lu) and determined their crystal structures in detail through the Rietveld analysis for the powder X-ray diffraction data. Mössbauer spectrum measurements were performed in order to determine the oxidation state of europium ions and to obtain the information about the coordination circumstances around the Eu ion. Magnetic susceptibilities of EuLn_2O_4 compounds were measured in the temperature range between 1.8 and 400 K in order to elucidate their magnetic properties.

2. Experimental

2.1. Sample preparation

The EuLn_2O_4 (Ln = Gd, Dy–Yb) were prepared by heating 1:1 mixtures of EuO and Ln_2O_3 in an evacuated quartz tube at 1373 K for a day. The EuO was prepared by heating mixtures of Eu metal and Eu_2O_3 in an evacuated quartz tube at 1073 K for a day.

* Corresponding author. Fax: +81 11 706 2702.
E-mail address: hinatsu@sci.hokudai.ac.jp (Y. Hinatsu).

0022-4596/$ - see front matter © 2009 Elsevier Inc. All rights reserved.
doi:10.1016/j.jssc.2009.04.001

2.2. X-ray diffraction analysis

Powder X-ray diffraction profiles were measured using a Rigaku Multi-Flex diffractometer with Cu$K\alpha$ radiation equipped with a curved graphite monochromator. The data were collected by step-scanning in the angle range of $10^\circ \leqslant 2\theta \leqslant 120^\circ$ at a 2θ step-size of 0.02°. The X-ray diffraction data were analyzed by the Rietveld technique, using the programs RIETAN2000 [10].

2.3. Magnetic susceptibility measurements

The temperature dependence of the magnetic susceptibility was measured in an applied field of 0.1 T over the temperature range of $1.8\,K \leqslant T \leqslant 400\,K$, using a SQUID magnetometer (Quantum Design, MPMS5S). The susceptibility measurements were performed under both zero-field-cooled (ZFC) and field-cooled (FC) conditions. The former was measured upon heating the sample to 400 K under the applied magnetic field of 0.1 T after zero-field cooling to 1.8 K. The latter was measured upon cooling the sample from 400 to 1.8 K at 0.1 T.

2.4. ^{151}Eu Mössbauer spectroscopy measurements

The ^{151}Eu Mössbauer spectra were measured with a Mössbauer spectrometer VT-6000 (Laboratory Equipment Co.) in the constant acceleration mode using a radiation source $^{151}SmF_3$ (1.85 GBq). The spectrometer was calibrated with a spectrum of α-Fe at room temperature. The γ-rays were detected with a NaI scintillation counter. Europium trifluoride (EuF_3) was used as a reference standard for the isomer shift (IS). The sample was wrapped in an aluminum foil so as to have its average surface density of $10\,mg(Eu)\,cm^{-2}$.

3. Results and discussion

3.1. Preparation and crystal structure

We could successfully prepare a series of EuLn_2O_4 compounds with Ln = Gd, Dy–Lu. A representative powder X-ray diffraction profile is shown in Fig. 1 for $EuYb_2O_4$. The observed diffraction peaks were indexed on an orthorhombic cell with the space group *Pnma*. The X-ray diffraction data for all the compounds studied in this study were analyzed by the Rietveld method. The refined lattice parameters and reliability factors for EuLn_2O_4 prepared in this study are listed in Table 1. We attempted to prepare EuLn_2O_4 with larger Ln. However, a single phase of EuLn_2O_4 was not obtained for any of Ln = La–Nd. We will discuss this point from the bond valence sum (BVS) calculation using the refined structural parameters, later. Fig. 2 shows the variation of lattice parameters with the ionic radius of Ln^{3+} ion in the six-coordination. The lattice parameters (a, b, and c) increase with the ionic radius of Ln^{3+} ion. The refined structural parameters of $EuLu_2O_4$ are listed in Table 2. For other compounds with Ln = Gd, Dy–Yb, the structural parameters are summarized in Supplementary tables.

Fig. 3(a) shows a schematic crystal structure of EuLn_2O_4. In this structure, Ln ions occupy two different crystallographic sites (Ln1 and Ln2) and are coordinated by six oxide ions in an octahedral manner. The $Ln1O_6$ and $Ln2O_6$ octahedra both form the zigzag chains along the b-axis. These chains connect with each other and build up the honeycomb-like framework. The Eu ions locate in the tunnel of the honeycomb structure.

The average bond lengths (Ln1–O, Ln2–O, and Eu–O) were calculated using the refined structural parameters and they were plotted against the ionic radius of Ln^{3+} in Fig. 4. With increasing the size of Ln^{3+} ion, both the lengths Ln1–O and Ln2–O increased. In addition, the Eu–O distances also increased, which is due to the result that the hexagonal tunnel is formed by the honeycomb-like linkage of LnO_6 octahedra.

The bond valence sums [11,12] for Ln and Eu ions were calculated using the refined structural parameters, and they are listed in Table 3. Fig. 5 shows the variation of BVS values against

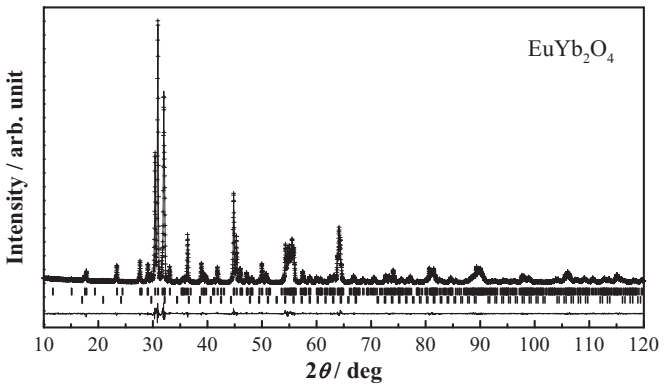

Fig. 1. Powder X-ray diffraction profile of $EuYb_2O_4$. The calculated and observed profiles are shown on the top solid line and cross markers, respectively. The vertical marks in the middle show positions calculated for Bragg reflections. The second vertical marks show positions for an impurity of Yb_2O_3 (the content is 1 mol%). The lower trace is a plot of the difference between calculated and observed intensities.

Table 1
Lattice parameters and reliability factors for EuLn_2O_4.

Ln	*a* (Å)	*b* (Å)	*c* (Å)	R_{wp} (%)	R_I (%)	R_e (%)
Gd	10.0986(4)	3.4769(1)	12.0439(5)	7.34	1.02	6.45
Dy	10.0669(3)	3.4321(1)	11.9374(3)	7.52	0.92	6.34
Ho	10.0481(3)	3.4107(1)	11.9040(3)	6.52	1.16	5.58
Er	10.0260(2)	3.3919(1)	11.8628(3)	5.93	0.88	4.90
Tm	9.9896(2)	3.3785(1)	11.8126(3)	5.63	1.24	3.43
Yb	9.9699(2)	3.3564(1)	11.7642(2)	7.02	1.03	5.11
Lu	9.9651(2)	3.3415(1)	11.7478(2)	6.30	0.90	4.85

Definitions of reliability factors R_{wp}, R_I, and R_e are given as follows: $R_{wp} = [\sum w(|F_o| - |F_c|)^2 / \sum w|F_o|^2]^{1/2}$, $R_I = \sum |I_{ko} - I_{kc}| / \sum I_{ko}$, and $R_e = [(N-p)/\sum_i w_i y_i^2]^{1/2}$.

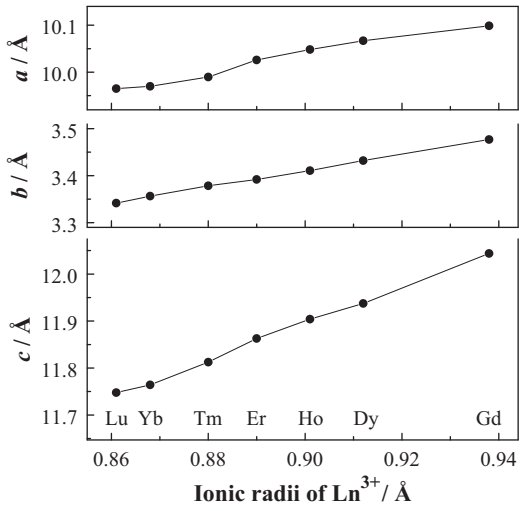

Fig. 2. Variation of lattice parameters for EuLn_2O_4 with the ionic radius of Ln^{3+} ion.

Table 2
Structural parameters for $EuLu_2O_4$.

Atom	Site	x	y	z	B (Å^2)
Eu	4c	0.7532(1)	1/4	0.6504(1)	0.39(2)
Lu1	4c	0.4218(1)	1/4	0.1092(1)	0.30(2)
Lu2	4c	0.4254(1)	1/4	0.6121(1)	0.30
O1	4c	0.2108(9)	1/4	0.1699(7)	0.58(5)
O2	4c	0.1259(8)	1/4	0.4810(8)	0.58
O3	4c	0.5191(9)	1/4	0.7835(7)	0.58
O4	4c	0.4223(9)	1/4	0.4244(7)	0.58

Note: Space group *Pnma*; $a = 9.9651(2)$ Å, $b = 3.3415(1)$ Å, $c = 11.7478(2)$ Å, $R_{wp} = 6.30\%$, $R_I = 0.90\%$, and $R_e = 4.85\%$.

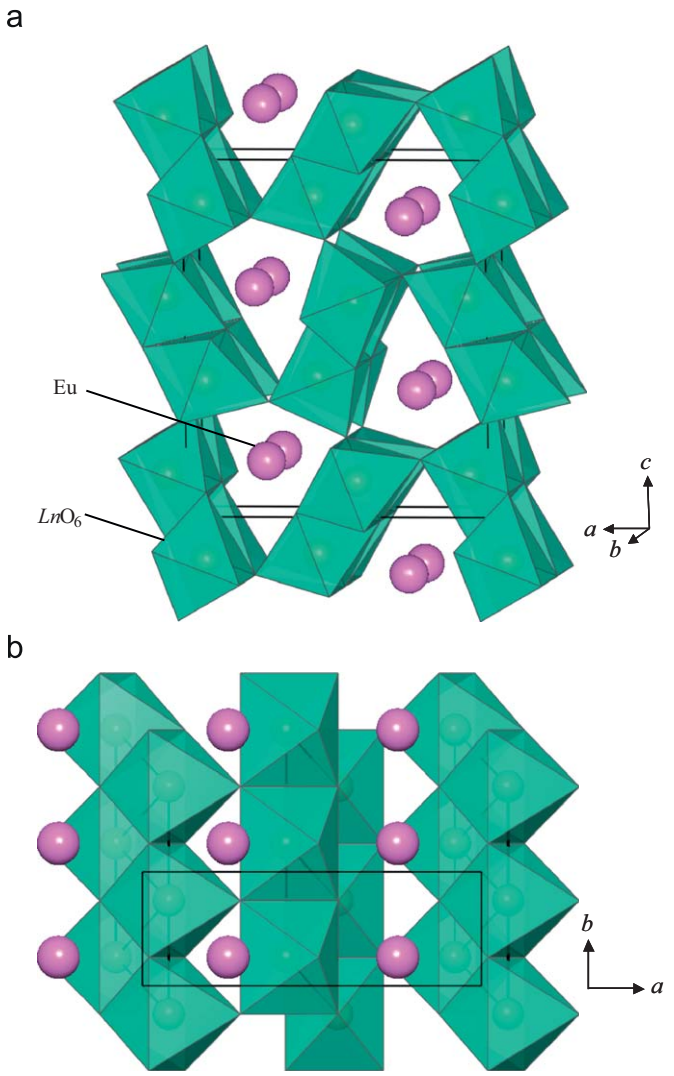

Fig. 3. (a) The schematic crystal structure of EuLn_2O_4. (b) Structure of EuLn_2O_4 viewed from the c-axis. The Eu atoms form magnetic chains parallel to the b-axis (see text).

the ionic radius of Ln^{3+} ion in the EuLn_2O_4. The values for the Ln ion are almost constant (~3.0) and they are reasonable for trivalent ions. Those for the Eu ions are close to 2.0 for Ln = Er–Lu compounds. However, they are actually decreasing with increasing the radius of Ln^{3+}. From Fig. 5, it is estimated that for the large size of Ln ions (Ln = La–Nd), the BVS values should be calculated to be much smaller than 2. This accounts for the difficulty in preparing EuLn_2O_4-type compounds with the large

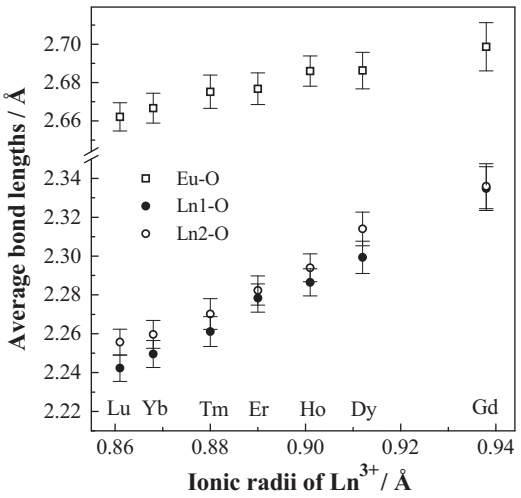

Fig. 4. Average Ln–O and Eu–O bond lengths of EuLn_2O_4.

Table 3
The BVS values of Ln(1), Ln(2), and Eu ions for EuLn_2O_4.

	$EuGd_2O_4$	$EuDy_2O_4$	$EuHo_2O_4$	$EuEr_2O_4$	$EuTm_2O_4$	$EuYb_2O_4$	$EuLu_2O_4$
Ln(1)	2.95	3.00	2.99	2.94	2.98	2.96	2.91
Ln(2)	2.92	2.86	2.92	2.89	2.92	2.88	2.79
Eu	1.78	1.83	1.83	1.88	1.88	1.93	1.96

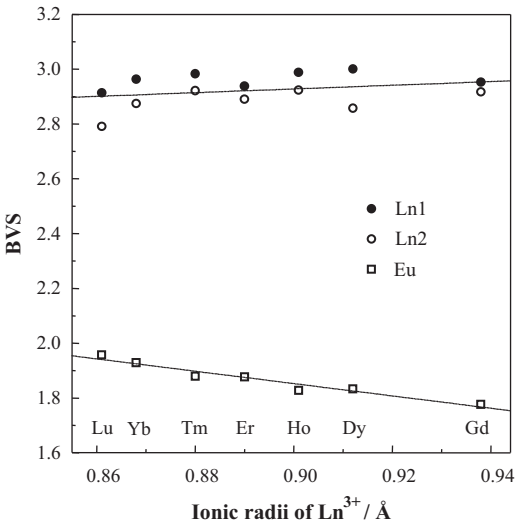

Fig. 5. Variation of bond valence sum (BVS) for Ln1, Ln2, Eu ions in EuLn_2O_4 against the ionic radius of Ln^{3+} ion.

size of Ln ions, i.e., the size of the tunnel of the honeycomb structure becomes too large to stabilize the Eu^{2+} ions in this structure.

Table 4 lists the atomic distance between Eu–Eu for all the EuLn_2O_4 compounds. The distance between the Eu atoms in the tunnel (along the crystallographic b-axis, see Fig. 3) is much smaller than the other Eu–Eu distances. The Eu atoms form "chains" parallel to the b-axis, with a spacing of 3.3–3.4 Å between atoms on a chain, and with two neighboring Eu chains separated by 5.5–6.5 Å. Therefore, there exists a strong magnetic interaction between the Eu atoms in the chain.

Table 4
The Eu–Eu distances (Å) in EuLn_2O_4.

	$EuGd_2O_4$	$EuDy_2O_4$	$EuHo_2O_4$	$EuEr_2O_4$	$EuTm_2O_4$	$EuYb_2O_4$	$EuLu_2O_4$
Eu chain							
(×2)	3.48	3.43	3.41	3.39	3.38	3.36	3.34
Neighboring Eu chain							
(×2)	5.61	5.58	5.57	5.54	5.53	5.51	5.50
(×4)	6.27	6.21	6.19	6.17	6.14	6.12	6.11

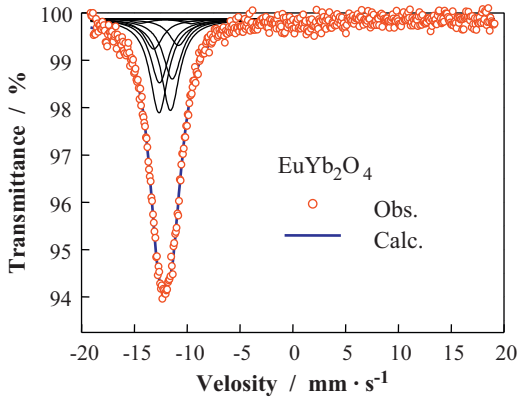

Fig. 6. ^{151}Eu Mössbauer spectrum of $EuYb_2O_4$ measured at room temperature.

3.2. ^{151}Eu Mössbauer spectrum

Fig. 6 shows the ^{151}Eu Mössbauer spectrum for $EuYb_2O_4$. One absorption peak appeared at $\delta = -12.09$ mm/s, showing strongly that the Eu ions are in the divalent state. In addition, a very weak absorption may be observed at about $\delta = 0$ mm/s, which is due to Eu^{3+}. Since the ground state of Eu^{3+} is non-magnetic ($^7F_0$ ($J = 0$)), its contribution to the magnetic properties of EuLn_2O_4 compounds (Eu^{2+}: $J = 7/2$) is negligible. Because of the low symmetry of the Eu site in $EuYb_2O_4$, an electric field gradient tensor should exist at this site. The non-zero quadrupole interaction is expected at the Eu site. The quadrupole Hamiltonian is given by

$$H_Q = \frac{e^2qQ}{4I(2I-1)}\left(3I_z^2 - I(I+1) + \eta(I_x^2 + I_y^2)\right) \quad (1)$$

where I is the nuclear spin, Q is the quadrupole moment, $eq = V_{zz}$, and $\eta = (V_{xx}–V_{yy})/V_{zz}$ (V_{ii} is the electric gradient tensor). Actually, the spectrum exhibited a slightly asymmetric line ($\eta \neq 0$). It is impossible to fit such a spectrum with a single Lorentzian line because of the distortion due to the quadrupole interaction. The 12 possible transitions (eight allowed transitions and four forbidden transitions) due to a quadrupole interaction were taken into account; the observed data were fitted with the sum of these Lorentzian lines. In order to derive these Lorentzian equations, the results by Shenoy and Dunlap were used [13] and the ratio of the excited and ground state quadrupole moments ($R_Q = Q_e/Q_g$) was taken as 1.312 [14]. The fitting parameters, the isomer shift, the quadrupole coupling constant (QS) and the asymmetry parameter (η) are determined for EuLn_2O_4 compounds, and they are listed in Table 5.

In Fig. 7, the isomer shifts of Eu^{2+} in EuLn_2O_4 are plotted against the average bond length of Eu–O. The isomer shift increases linearly with decreasing the bond length, which is due to the increment of the s electron density at the ^{151}Eu nucleus with decreasing the Eu–O bond length. Similar trend has been reported for EuLn_2S_4 [15].

Table 5
Mössbauer parameters for EuLn_2O_4.

Ln	IS (mm s^{-1})	QS (mm s^{-1})	η
Gd	−12.29(1)	8.2(1)	0.40(4)
Dy	−12.23(1)	7.6(1)	0.56(3)
Ho	−12.15(1)	7.3(1)	0.72(2)
Er	−12.12(1)	7.3(1)	0.85(3)
Tm	−12.09(1)	7.5(1)	0.89(4)
Yb	−12.09(1)	6.9(1)	0.95(8)
Lu	−12.10(1)	7.5(1)	1.0(1)

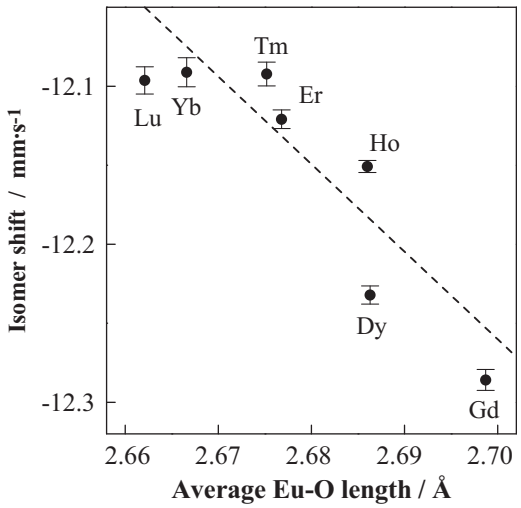

Fig. 7. Isomer shift of Eu^{2+} for EuLn_2O_4 against the average bond length of Eu–O.

3.3. Magnetic properties

3.3.1. $EuLu_2O_4$

Temperature dependence of the magnetic susceptibility of $EuLu_2O_4$ is shown in Fig. 8(a). An antiferromagnetic transition was observed at 5.7 K. Because the Lu^{3+} ion is diamagnetic, only the Eu^{2+} ion contributes to the magnetic properties of $EuLu_2O_4$. By applying the Curie–Weiss law to the susceptibility in the temperature range between 200 and 400 K, the effective magnetic moment was determined to be 7.94μ_B, which is in accordance with the moment for Eu^{2+} (7.94μ_B). Although the magnetic susceptibility vs. temperature curve shows the existence of the antiferromagnetic interaction in $EuLu_2O_4$, the Weiss constant determined is positive, 15.7 K, indicating that the predominant magnetic interaction between Eu^{2+} ions is ferromagnetic at low temperatures. Fig. 8(b) shows the variation of the reciprocal magnetic susceptibility of $EuLu_2O_4$ against temperature. The positive Weiss constant shows the existence of the ferromagnetic interaction between Eu ions.

Fig. 9 shows the field dependence of the magnetization for $EuLu_2O_4$ measured at 1.8 K. The magnetization linearly increases and then reaches an almost constant value (7μ_B). This value is in good agreement with the saturation moment theoretically expected for the Eu^{2+} ion. These results suggest that the magnetic properties at low temperatures are determined by the strongly magnetic ions Eu^{2+}. It is reasonable to assume that the strongest interactions (ferromagnetic) couple nearest neighbors of Eu^{2+} ions, and that weaker interactions (antiferromagnetic) couple more distant neighbors to give, over all, an antiferromagnetic ground state. Considering the crystal structure, neighboring ferromagnetic Eu^{2+} chains interact weakly to give an antiferromagnetic ground state, as indicated in Fig. 10.

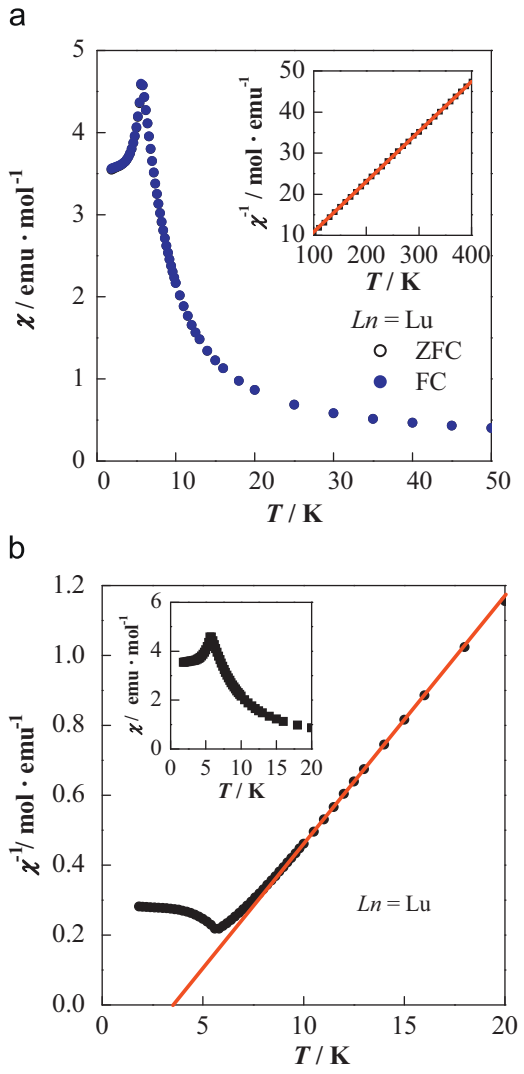

Fig. 8. (a) Temperature dependence of the magnetic susceptibility of $EuLu_2O_4$ below 50 K. The inset shows the reciprocal susceptibility vs. temperature curve in the temperature range between 100 and 400 K. The solid line is the Curie–Weiss fitting. (b) The reciprocal susceptibility vs. temperature curve below 20 K. The solid line is the Curie–Weiss fitting in the low temperature region. The Weiss constant is still positive.

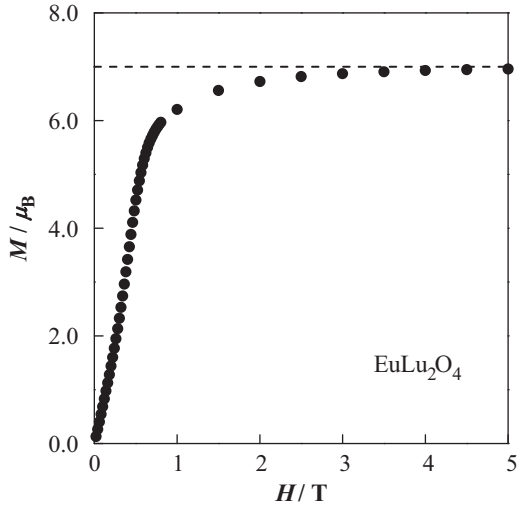

Fig. 9. Field dependence of magnetization of $EuLu_2O_4$ measured at 1.8 K.

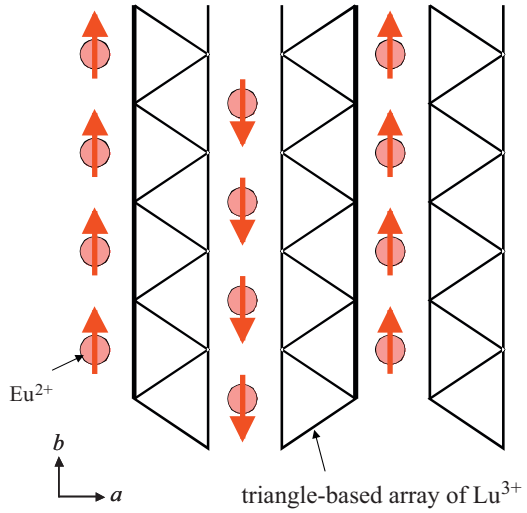

Fig. 10. Neighboring chains of Eu^{2+} in $EuLu_2O_4$ viewed from almost the *c*-axis. Arrows show proposed magnetic structure. Between Eu^{2+} chains, triangle-based array of Lu ions is located. The Lu ions are omitted from the magnetic structure, because they are diamagnetic.

The ferromagnetic state in the high field is produced by reversing half of the chains to bring all of the Eu^{2+} spins into alignment with the magnetic field. The critical field is low, ~2 T, because the relatively weak interchain interactions are affected by the ferromagnetic transition.

3.3.2. *$EuHo_2O_4$ and other Ln = Gd, Dy, Er and Tm compounds*

The situation for the $EuLn_2O_4$ (*Ln* = Gd–Tm) is quite different from that for $EuLu_2O_4$, because these Ln^{3+} ions are paramagnetic with large magnetic moments. Temperature dependence of the magnetic susceptibility for $EuHo_2O_4$ is shown in Fig. 11(a). A clear antiferromagnetic transition was observed at 4.2 K. The effective magnetic moment determined from the Curie–Weiss law is $16.89\mu_B$. The effective magnetic moment for this compound is given by the following equation:

$$\mu_{eff}^2 = [\mu_{eff}]_{Eu^{2+}}^2 + 2[\mu_{eff}]_{Ho^{3+}}^2. \quad (2)$$

The moment experimentally obtained is almost consistent with the moment calculated by this equation with using the free ion values of Eu^{2+} and Ho^{3+} ions ($16.97\mu_B$). The Weiss constant is −14.6 K, which indicates that the antiferromagnetic interactions are predominant. This result is contrastive with the case for $EuLu_2O_4$. Fig. 11(b) shows the reciprocal susceptibility vs. temperature curve below 20 K. For isomorphous $SrLn_2O_4$ (*Ln* = Gd–Yb) compounds, their Weiss constants were reported to be −10 to −99 K [8]. Although the large negative Weiss constants indicate that the magnetic interactions between *Ln* ions are antiferromagnetic, none of the samples showed the sharp features associated with long-range magnetic ordering in their susceptibility vs. temperature curves. The results were interpreted qualitatively with the magnetically frustrated model, and were due to the triangle-based array of *Ln* atoms (see Fig. 12(a)). In the case of $EuHo_2O_4$, in addition to the Eu^{2+} ions, Ho^{3+} ions also have a large magnetic moment. Therefore, the magnetic interactions between Eu and Ho ions should be very important. Furthermore, the distance between the nearest Eu–Ho atoms is 3.31 Å, which is shorter than that between the nearest Eu–Eu atoms (3.41 Å).

Fig. 13 shows the field dependence of the magnetization of $EuHo_2O_4$. Due to the strong magnetic interaction between Eu^{2+} and Ho^{3+} ions, the trend of saturation of the magnetization was not observed even at $H = 5$ T.

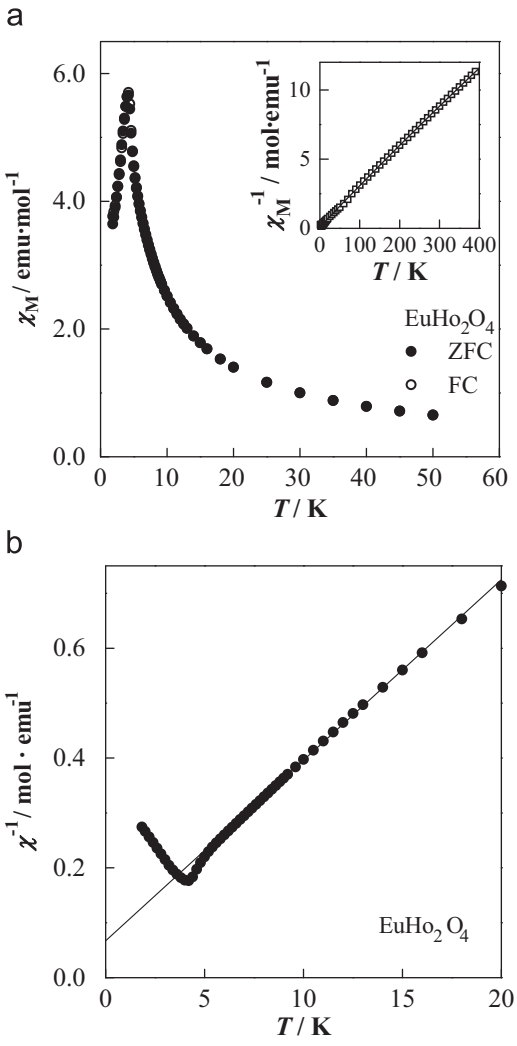

Fig. 11. (a) Temperature dependence of the magnetic susceptibility of $EuHo_2O_4$. The inset shows the reciprocal susceptibility vs. temperature curve. The solid line is the Curie–Weiss fitting. (b) The reciprocal susceptibility vs. temperature curve below 20 K. The Weiss constant is negative.

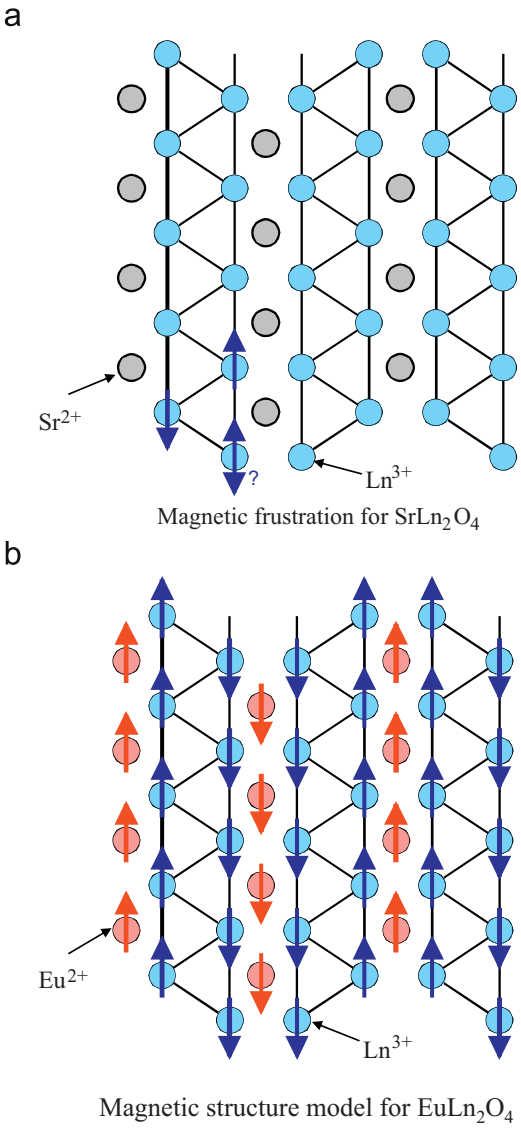

Fig. 12. (a) Magnetic frustration for $SrLn_2O_4$. (b) Proposed magnetic structure for $EuLn_2O_4$.

3.3.3. $EuLn_2O_4$ (Ln = Gd, Dy, Er, Tm, Yb)

Figs. 14(a) and (b) show the temperature dependence of magnetic susceptibility for $EuGd_2O_4$ and $EuDy_2O_4$, respectively. All the other $EuLn_2O_4$ compounds (Ln = Gd, Dy, Er, Tm, Yb) showed an antiferromagnetic transition at 4.7–6.3 K. The effective magnetic moments, Weiss constants and Neel temperatures are listed in Table 6. The effective magnetic moments for $EuLn_2O_4$ obtained experimentally are comparable to those calculated from Eq. (2). The Weiss constants for $EuLn_2O_4$ (Ln = Gd–Yb) compounds are negative, whereas that for Ln = Lu compound is positive.

In the case of $EuLn_2O_4$ (Ln = Gd–Yb), both the Eu^{2+} and Ln^{3+} ions have a large magnetic moment, and not only ferromagnetic interactions between nearest Eu^{2+} ions, but also magnetic interactions between Eu^{2+} and Ln^{3+} ions should greatly contribute to the magnetic properties of $EuLn_2O_4$ (Ln = Gd–Yb). Due to the magnetic interaction of ferromagnetically aligned Eu^{2+} ions with the Ln^{3+} ions, magnetic frustration by the triangle geometry of Ln^{3+} ions disappears. Relatively strong magnetic interaction between Eu^{2+} and Ln^{3+} ions would overcome the geometrically

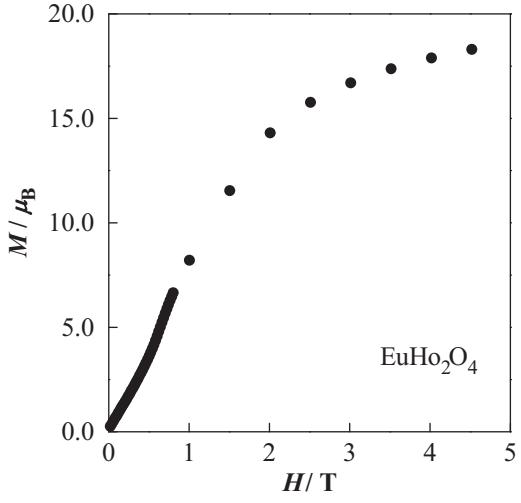

Fig. 13. Field dependence of magnetization of $EuHo_2O_4$ measured at 1.8 K.

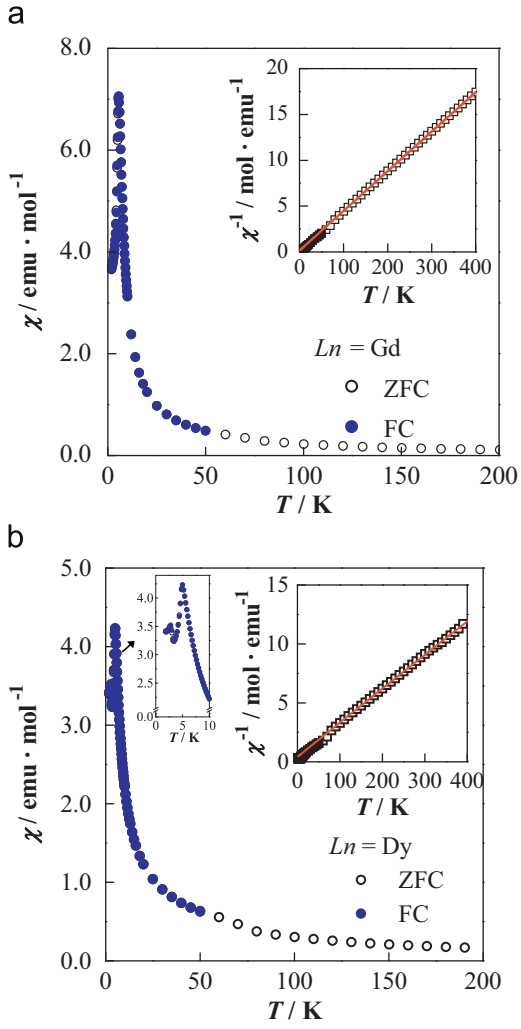

Fig. 14. (a) Temperature dependence of the magnetic susceptibility of $EuGd_2O_4$ below 200 K. The inset shows the reciprocal susceptibility vs. temperature curve. The solid line is the Curie–Weiss fitting. (b) Temperature dependence of the magnetic susceptibility of $EuDy_2O_4$ below 200 K. An upturn in the susceptibility at 2.5 K below T_N may be ascribed to another magnetic ordering of Dy^{3+} moments. The inset shows the reciprocal susceptibility vs. temperature curve. The solid line is the Curie–Weiss fitting.

magnetic frustration of triangllly aligned Ln^{3+} ions, and $EuLn_2O_4$ compounds show the predominantly antiferromagnetic behavior. We present, as one example, the proposed magnetic structure for $EuLn_2O_4$ (Ln = Gd–Yb) as shown in Fig. 12(b).

Table 6
The effective magnetic moments (μ_{eff}: experimental, μ_{cal}: calculated) per formula unit, Weiss constants, and Néel temperatures for $EuLn_2O_4$.

Ln	μ_{eff} (μ_B)	μ_{cal} (μ_B)	θ (K)	T_N (K)
Gd	13.62(1)	13.75	−4.8(3)	5.6
Dy	16.74(5)	17.02	−18(2)	5.0
Ho	16.89(3)	16.97	−14.6(6)	4.2
Er	15.44(2)	15.70	−4.4(4)	4.7
Tm	13.74(4)	13.32	−26(2)	5.4
Yb	10.42(2)	10.21	−32(2)	6.3
Lu	7.94(2)	7.94	15.7(7)	5.7

Acknowledgment

This work was supported by Grant-in-aid for Scientific Research, No. 20550052 from the Ministry of Education, Science, Sports, and Culture of Japan.

Appendix A. Supplementary material

Supplementary data associated with this article can be found in the online version at doi:10.1016/j.jssc.2009.04.001.

References

[1] L. Holmes, M. Schieber, J. Appl. Phys. 37 (1966) 968–969.
[2] O. De Pous, L. Albert, J.-C. Achard, C. R. Seances Acad. Sci. Ser. C Sci. Nat. 276 (1973) 763–766.
[3] A.A. Samokhvalov, Yu.N. Morozov, V.G. Bamburov, N.V. Volkenshtein, T.D. Zotov, Fiz. Tverd. Tela (St.–Peterb.) 10 (1968) 2206–2208.
[4] A.A. Samokhvalov, Yu.N. Morozov, V.G. Bamburov, N.V. Arbuzova. T.I., Fiz. Tverd. Tela (St.–Peterb.) 13 (1971) 2683–2686.
[5] L.M. Lopato, A.V. Shevchenko, I.S. Kir'yakova, Dopov. Akad. Nauk Ukr. RSR, Ser. B 30 (1968) 826–829.
[6] J.P. Attfield, Nature 343 (1990) 46–49.
[7] G.B. Jin, E.S. Choi, R.P. Guertin, T.E. Albrecht–Schmitt, J. Solid State Chem. 181 (2008) 14–19.
[8] H. Karunadasa, Q. Huang, B.G. Ueland, J.W. Lynn, P. Schiffer, K.A. Regan, R.J. Cava, Phys. Rev. B 71 (2005) 144414.
[9] Y. Doi, W. Nakamori, Y. Hinatsu, J. Phys. Condens. Matter 18 (2006) 333–344.
[10] F. Izumi, T. Ikeda, Mater. Sci. Forum 198 (2000) 321–324.
[11] I.D. Brown, A. Altermatt, Acta. Crystallogr. Sect. B 41 (1985) 244–247.
[12] N.E. Brese, M. O'Keeffe, Acta Crystallogr. Sect. B 47 (1991) 192–197.
[13] G.K. Shenoy, B.D. Dunlap, Nucl. Instrum. Methods 71 (1969) 285.
[14] J.G. Stevens, J.W. Robinson (Eds.), Handbook of Spectroscopy, vol. 3, CRC Press, Boca Raton FL, 1981 p. 464.
[15] O. Berkooz, J. Phys. Chem. Solids 30 (1969) 1763–1767.